Geophysical Research Letters

RESEARCH LETTER
10.1029/2018GL080320

Separating the North and South Pacific Meridional Modes Contributions to ENSO and Tropical Decadal Variability

Giovanni Liguori[1,2] **and Emanuele Di Lorenzo**[1]

[1]School of Earth and Atmospheric Sciences, Georgia Institute of Technology, Atlanta, GA, USA, [2]ARC Centre of Excellence for Climate Extremes, School of Earth, Atmosphere and Environment, Monash University, Melbourne, Victoria, Australia

Key Points:
- The absence of NPMM variability in CESM leads to a significant reduction of the tropical interannual variability (~35%)
- The absence of the SPMM does not impact the ENSO spectrum but leads to a significant reduction of the decadal variability (~30%)
- The NPMM and SPMM modes energize the tropical variance independently on interannual and decadal timescale respectively

Supporting Information:
- Figure S1

Correspondence to:
G. Liguori,
giovanni.liguori@monash.edu

Citation:
Liguori, G., & Di Lorenzo, E. (2019). Separating the North and South Pacific Meridional Modes contributions to ENSO and tropical decadal variability. *Geophysical Research Letters*, *46*, 906–915. https://doi.org/10.1029/2018GL080320

Received 7 SEP 2018
Accepted 19 DEC 2018
Accepted article online 3 JAN 2019
Published online 23 JAN 2019

Abstract North and South Pacific Meridional Modes (NPMM and SPMM) are known precursors of El Niño–Southern Oscillation (ENSO) and Tropical Pacific decadal variability (TPDV). However, the relative importance of these precursors and the timescale on which they impact the tropics remain unclear. Using a 30-member ensemble of the Community Earth System Model as the control climate, we generate two additional members where the NPMM and SPMM are selectively suppressed. We find that both meridional modes energize the tropical variance independently on different timescales. The absence of NPMM leads to a significant reduction of the tropical interannual variability (~35%), while the absence of the SPMM has no appreciable impact on ENSO but significantly reduces the TPDV (~30%). While the relative importance of the NPMM and SPMM may be model dependent, the stochastic atmospheric variability in the extratropics that energizes the meridional modes emerges as a key source of TPDV.

Plain Language Summary El Niño–Southern Oscillation (ENSO) and the Tropical Pacific decadal variability (TPDV) exert a strong influence over the climate of large parts of the world. To understand and predict tropical Pacific variability, it is necessary to study all those oceanic and atmospheric processes that act as triggers and energizers of ENSO and TPDV, also referred to as the *precursor dynamics*. The North and South Pacific Meridional Modes (NPMM and SPMM) are well-known precursors of ENSO and TPDV; however, their relative importance and the timescale on which they exert their influence remain unclear. We use a climate model to perform simulations where either NPMM or SPMM variability are selectively suppressed. We find that the absence of NPMM leads to a significant reduction of ENSO (~35%), while the absence of the SPMM has no appreciable impact on ENSO but significantly reduces the TPDV (~30%). The NPMM and SPMM modes impact the tropical variance independently on interannual and decadal timescale, respectively.

1. Introduction

Sea surface temperatures (SSTs) in the equatorial Pacific associated with El Niño–Southern Oscillation (ENSO) exert significant control over the interannual variability of the basin climate (e.g., Alexander et al., 2002; Harrison & Larkin, 1998; McPhaden et al., 2006), which drives major societal and economic impacts (e.g., Adams et al., 1999; Berry & Okulicz-Kozaryn, 2008; Cashin et al., 2017; Fisman et al., 2016). To first order, ENSO can be thought of as a collection of modes that are amplified along the zonal equatorial plane by positive coupled feedbacks between the ocean and atmosphere (Bjerknes, 1969; Jin, 1997; Suarez & Schopf, 1988). To understand and predict ENSO, it is necessary to study all those oceanic and atmospheric processes that act prior to its extreme manifestation—the ENSO precursor dynamics. While important ENSO precursors (e.g., westerly wind burst and Madden-Julian oscillations) act along the equator and rely on equatorial wave dynamics (Fedorov, 2002; Kessler & Kleeman, 2000; McPhaden, 1999; McPhaden & Yu, 1999; Zavala-Garay et al., 2005), extratropical precursors, such as North and South Pacific Meridional Modes (NPMM, Chiang & Vimont, 2004, and SPMM, H. Zhang et al., 2014), have also been found to be very effective in energizing both ENSO (Alexander et al., 2010; Chang et al., 2007; Larson & Kirtman, 2013, 2014; Thomas & Vimont, 2016; You & Furtado, 2017; L. Zhang, Chang, Ji, 2009; L. Zhang, Chang, & Tippett, 2009) and tropical Pacific decadal variability (TPDV; Di Lorenzo et al., 2015; Liguori & Di Lorenzo, 2018; H. Zhang et al., 2014). SPMM and NPMM are coupled ocean-atmosphere modes of variability in the tropical and subtropical Pacific Ocean that rely on a

positive feedback between the wind-induced evaporation and the underlying SST anomalies (SSTa; i.e., wind-evaporation-SST [WES] feedback; Xie & Philander, 1994).

Using reanalysis data sets, the spatial signature of the extratropical dynamics affecting ENSO is revealed by performing a simple analysis where the first principal component (PC1) of October-November-December (OND) mean SSTa in the equatorial Pacific [12°S to 12°N; i.e., ENSO index, *Ei*) is regressed onto preceding SST and sea level pressure (SLP) anomalies of January-December-February (JFM) of the same year. In the subtropics, the SST precursor shows a clear signature of the NPMM and SPMM (Figure 1c) that is consistent with the extratropical SLP precursor (Figure 1a), which shows low-pressure centers driving a weakening of the off-equatorial trade winds. This weakening of the trades is known to trigger several precursor dynamics, including the "seasonal foot-printing mechanism" (Vimont et al., 2001, 2003), the "trade wind charging" mechanism (Anderson, 2003; Anderson et al., 2013), and excitation of off-equatorial Rossby waves (Knutson & Manabe, 1998; Wang et al., 2003).

In the Northern Hemisphere, the atmospheric precursor pattern is characterized by the signature of the North Pacific Oscillation (NPO) mode (Linkin & Nigam, 2008; Rogers, 1981), known to be the optimal forcing for the NPMM. Similarly, in the Southern Hemisphere, the recently defined South Pacific Oscillation appears to be the optimal precursor of the SPMM (You & Furtado, 2017). The importance of these extratropical patterns in driving the tropical Pacific variability can be quantified using time indices for the north and south precursor patterns (i.e., *Ni* and *Si*; Figure 1), which are obtained by projecting extratropical JFM anomalies onto the precursor patterns ([150°E to 120°W, 12–50°N] for *Ni* and [160°E to 75°W, 12–50°S] for *Si*), to predict the OND ENSO index (i.e., *Ei*). For both SST and SLP, an important fraction of the interannual ENSO variance (~38% and ~35%, respectively, for SST and SLP) is predicted by linearly combining the contributions of *Ni* and *Si* time series (Figures 1g and 1h) which, in the observational record, are found to be largely independent ($R = 0.17$ and $R = 0.13$, for SST- and SLP-based indices, respectively; Ding et al., 2015).

Recent studies suggest that although independent, synergies between South and North Pacific precursors (e.g., NPMM and SPMM) may be important for amplifying the tropical variance (Ding et al., 2015; You & Furtado, 2017). However, it remains unclear from these studies what the relative importance of these precursors is, on what frequency their influence on the tropics is more effective (i.e., interannual vs. decadal timescales), and if destructive interference is also critical. While it is difficult to address these questions using exclusively observational analysis, experiments with coupled climate models can be designed to efficiently separate the contribution of ENSO precursor dynamics from the South and the North Pacific. Here we examine these dynamics in the Community Earth System Model (CESM) Large Ensemble (hereafter LENS) with a focus on the two dominant subtropical modes, the NPMM and SPMM, whose spatial signatures are highlighted by blue and red ellipses in the SST ENSO precursors shown in Figure 1c. In LENS, these precursor dynamics are spatially consistent with observations (Figure 1d) and present a stronger than observed connection with ENSO explaining 64% and 50% of the ENSO variance, respectively, for SST and SLP precursors (Figures 1g and 1h). However, given the large internal model variability, LENS can be considered consistent with the observations (Figures 1a, 1c, and 1e). In addition to the LENS simulations, we perform two extra LENS-like simulations in which either the NPMM or the SPMM variability is suppressed. These additional experiments, which differ from any other LENS member only for a regional restoring of SST, allow us to investigate the role and the relative importance of NPMM and SPMM in the tropical Pacific variability and establish the significance of the changes against the CESM ensemble. Using observational data sets and model simulations, our goals are to (1) identify the role of NPMM and SPMM precursors dynamics in the development of ENSO and (2) quantify the impact of both precursors in the statistics of the tropical Pacific variability from interannual to decadal timescale.

2. Data Sets and Methodology

We use two SST data sets, the Met Office Hadley Centre SST, version 1.1 (HadISST v1.1) data set (Rayner et al., 2003) and the National Oceanic and Atmospheric Administration Extended Reconstruction SST, version 3 (ERSST v3) product (Smith & Reynolds, 2005). HadISST v1.1 (ERSST v3) consists of monthly mean values from 1870 (1854) to the present on a 1° × 1° (2° × 2°) horizontal grid globally. SLP and 10-m wind components, *U* and *V*, are taken from the National Centers for Environmental Prediction-National Center

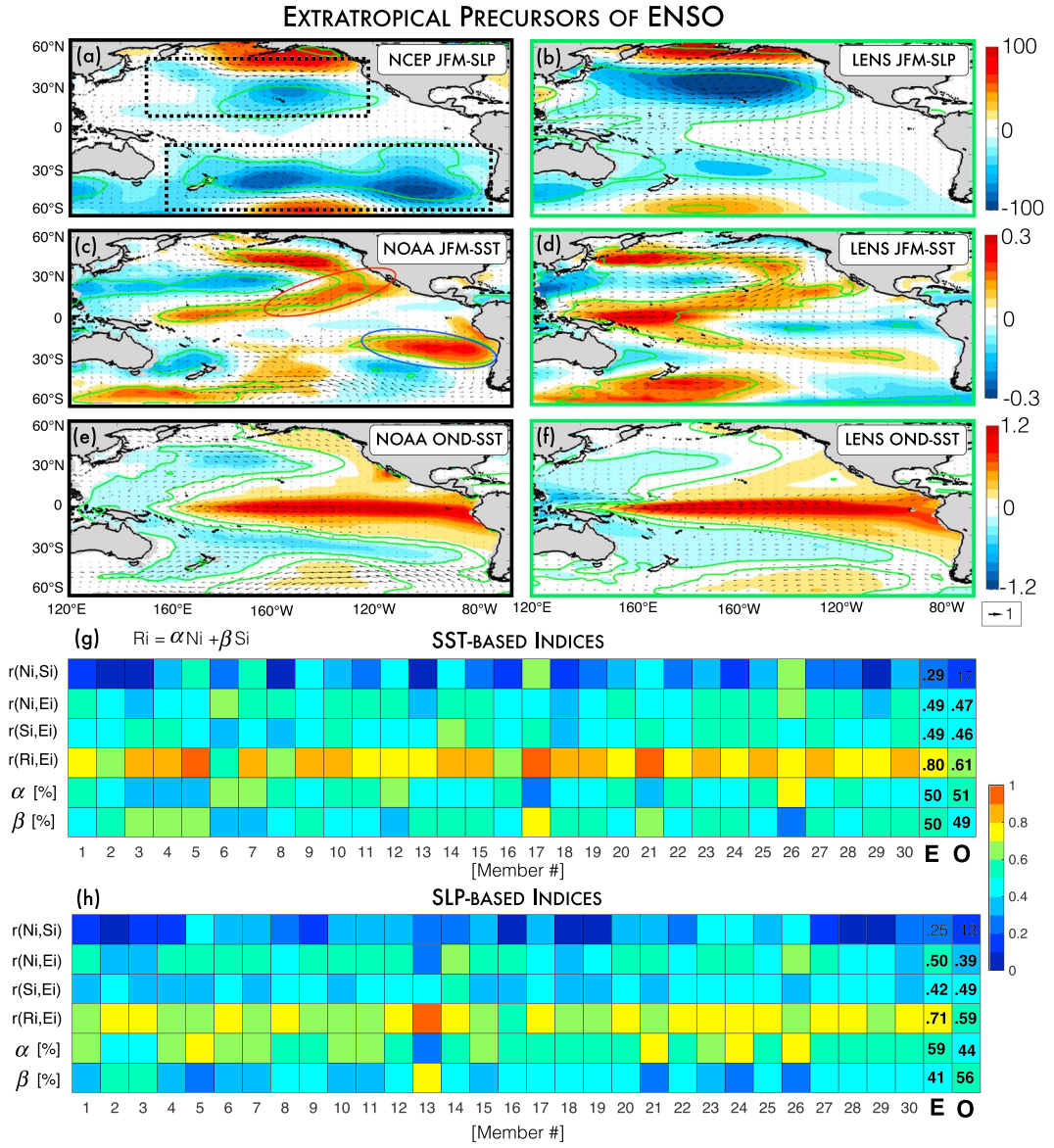

Figure 1. Precursor patterns of ENSO. Regression map between the SST-based OND ENSO index (i.e., *Ei*, see text for the definition) and (a) preceding JFM mean SLP anomalies, (c) preceding JFM mean SST anomalies, and (e) concurrent OND mean SST anomalies. Vectors indicate regression with wind components, observational data sets are from NOAA ERSST v3 (SST) and NCEP (SLP and wind components), the period analyzed is 1950–2005, and units are in degrees Celsius and Pascals. (b, d, and f) The same analysis done with LENS (ensemble mean). (g) Correlation coefficients between *Ei* and SST-based north and South Pacific precursors, *Ni* and *Si*, respectively (see text for definitions): Correlation between (first row) *Ni* and *Si*, (second row) *Ni* and *Ei*, (third row) *Si* and *Ei*, and (forth row) *Ei* with the best linear model, $Ri = \alpha Ni + \beta Si$. The relative weight (in percentage) of *Ni* (%α, fifth row) and *Si* (%β, sixth row) in the linear model is also shown. The correlation analysis is done for each LENS member (#1–30), the LENS ensemble mean (E), and the observational data sets (O). (h) As in (g) but for the SLP-based indices. The dash-lined boxes in (a) indicate the regions used to compute the projection indices *Ni* (upper box) and *Si* (lower box). The red-colored (blue-colored) ellipse in (c) indicates the area where the SST is restored for the noNPMM (noSPMM) experiment. Green contours in all the maps represent the 95% significance level based on a Student's *t* test. JFM = January-December-February; OND = October-November-December; ENSO = El Niño–Southern Oscillation; LENS = Large Ensemble; SLP = sea level pressure; SST = sea surface temperature; NOAA = National Oceanic and Atmospheric Administration; NCEP = National Centers for Environmental Prediction.

for Atmospheric Research reanalysis product (Kistler et al., 2001) and consist of monthly mean values from 1950 to present on a 2.5° × 2.5° horizontal grid globally. Except for Figure 1, which uses observation from 1950 to 2005, we analyzed the period of record 1920–2005 to match the historical segment of LENS simulations.

We analyze the first 30 members of the LENS for the period forced by historical greenhouse gas and aerosol concentrations (i.e., radiative forcing) that span 1920–2005. The simulation uses CESM version 1, with the Community Atmosphere Model, version 5 (CESM1-CAM5; Hurrell et al., 2013) at approximately 1° × 1° horizontal resolution in all model components. Throughout the manuscript, monthly mean anomalies are computed by removing the climatological seasonal cycle (i.e., long-term monthly mean of the record analyzed) from detrended fields. While for the observational data sets, detrended fields are obtained by removing the linear trend at each grid point, in LENS, they are obtained by removing at each grid point the ensemble mean, which is assumed to be the signal associated with the historical radiative forcing.

The NPMM (SPMM) pattern is obtained as leading maximum covariance analysis (MCA) of monthly mean SST and surface wind stress anomaly in the region [175°E to 95°W, 0° to 32°N] ([165–95°W, 32°S to 0°]) with ENSO removed by linear regression prior to the analysis. This calculation is similar to the one performed by Chiang and Vimont (2004) but computes the MCA on monthly mean value rather than on Spring anomalies, which introduces a preference on a specific season in the analysis. All the seasons in this manuscript are boreal seasons. It is noteworthy that both SPMM and NPMM are reproduced in LENS but with a different degree of realism. Specifically, the SPMM MCA exhibits a larger spatial bias with its center of action shifted westward with respect to observations (Figure S1 in the supporting information). The significance of the correlation coefficients throughout the study is estimated by computing empirical probability density functions (EPDFs) for the correlation coefficient of two red noise time series, which have the same lag-1 autoregressive coefficient of those estimated in the original signals. We assess the 99% significance levels using an EPDF obtained from 10,000 realizations of random red noise time series.

3. Coupling Experiment Design

To investigate the role and relative importance of NPMM and SPMM in driving ENSO and TPDV, we extend the CESM ensemble (i.e., LENS) by adding two extra members in which either the NPMM or the SPMM variability is suppressed by restoring the SST (2 days restoring factor) to the monthly mean climatology only in the region where these modes are most active (Figure S2). Although this strong restoring removes any SST variability longer than few days, and not exclusively the ones linked with meridional mode dynamics, we assume that statistically significant changes between the experiments and LENS are largely due to NPMM and SPMM dynamics. Hereafter, we will refer to these experiments as noNPMM and noSPMM for suppressed NPMM and suppressed SPMM, respectively. The regions where these modes are most active, which do not include the Tropical Pacific band between [10°S and 10°N], are identified by computing the LENS ensemble mean pattern of both NPMM and SPMM (Figure S2). These two extra members are highly comparable with LENS since they use same CESM code and configuration parameters, including numerical grids and radiative forcing. This is crucial given the very high internal variability that characterizes the model (e.g., Figures 1g and 1h) and presumably nature. Without a robust null hypothesis for the Pacific climate variability, as the one provided by LENS, it would not be possible to evaluate and assess the significance of the changes in the statistics of the Pacific climate driven by the suppression of the meridional modes variability. Specifically, the comparison with LENS becomes critical since we only dispone of a single run for each experiment, and thus, we are unable to characterize the internal variability for each experimental setup.

4. Impacts of NPMM and SPMM on ENSO

The impacts of NPMM and SPMM on ENSO is assessed by comparing noNPMM and noSPMM experiments with LENS. Except in the region where the SST restoring is applied, ENSO precursor patterns of the noSPMM experiment are largely unchanged. Both SLP and SST during the preceding JFM season are substantially similar to the ones of LENS. In the North Pacific, the NPO-like pattern emerges in the SLP (Figure 2b) and the North Pacific Gyre Oscillation-like pattern in the SST (Figure 2d). Major changes are instead visible in the precursor patterns for the noNPMM experiment. Specifically, the SLP precursor lacks the characteristic NPO-like pattern and the North Pacific is instead characterized by an Aleutian Low-like

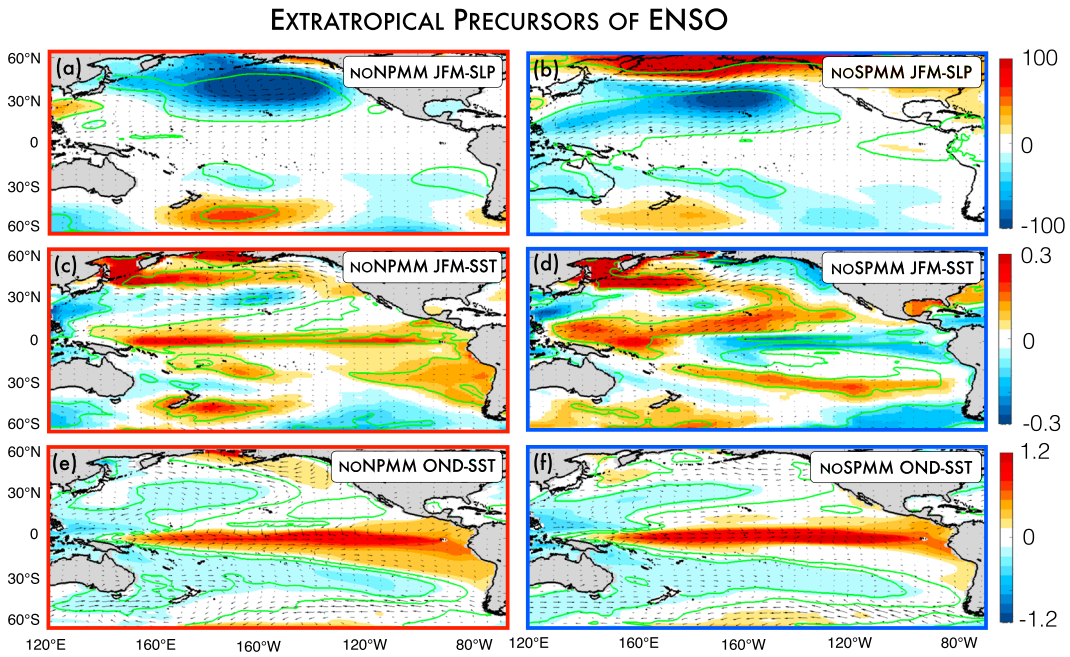

Figure 2. Precursor patterns of El Niño–Southern Oscillation in the Community Earth System Model experiments. Same as Figure 1 but for the experiments (a, c, and e) noNPMM and (b, d, and f) noSPMM. noNPMM = suppressed North Pacific Meridional Mode; noSPMM = suppressed South Pacific Meridional Mode; JFM = January-December-February; OND = October-November-December; SLP = sea level pressure; SST = sea surface temperature.

pattern. Even more remarkable are the changes in the SST precursor: While in both LENS and noSPMM the equator band presents an east-west dipole structure, in noNPMM this is replaced by a positive anomaly that extend across the whole basin. This remarkable change in ENSO precursors results in a significant reduction of ENSO activity during the succeeding OND season (Figure 2e).

To further explore the changes in tropical Pacific variance, we examine the first three empirical orthogonal functions (EOFs) of the SST in the tropics [120°E and 70°W, 25S° and 25°N], which in LENS track ENSO, the NPMM and the SPMM, respectively, for the first, the second, and the third modes (Figures 3a–3c). While this simple classification may appear as an over simplification, it is confirmed by the modal decomposition of noNPMM and noSPMM experiments (Figures 3d–3i). Specifically, the suppression of the NPMM variability results in a second mode (Figure 3e), which closely resembles the third mode of LENS (Figure 3c). Accordingly, the suppression of the SPMM variability only affects the third mode and leaves the first two leading modes mostly unchanged, which is analogous to LENS-EOF1 and LENS-EOF2. Although this three-mode framework explains well the equatorial variability in the CESM simulations (i.e., LENS, noNPMM, and noSPMM), its third mode, which represents the SPMM, differs substantially from the one computed using an observational product such as the HadISST (Figures 3j, 3k, and 3l). Moreover, using the North's rule (North et al., 1982), we find that the third and the second modes in HadISST are not completely separated, which makes the mode-by-mode comparison difficult between model and observation. The first mode, ENSO, is similar in both observation and CESM simulations. Nevertheless, the simulations all present a bias in the extension of the equatorial anomaly, which extends too far east (Figures 3a, 3d, and 3g).

The impacts of NPMM and SPMM on the equatorial SSTa spectrum is examined through the standard deviation (*SD*) of the monthly mean SSTa along the equatorial line (Figure 4a). When the NPMM is suppressed (i.e., noNPMM), there is a substantial reduction of tropical variance compared with LENS in the *SD* at all longitudes. This reduction, which for most latitudes (i.e., [170–110°W]) amounts to −35%, is highly statistically significant because all LENS members exhibit substantially higher values for the *SD*. However, it must be noted that LENS, and more generally this CESM version (i.e., version 1.1), presents a clear positive bias in the variance of the equatorial Pacific. When compared to LENS, the noSPMM experiment does not show any

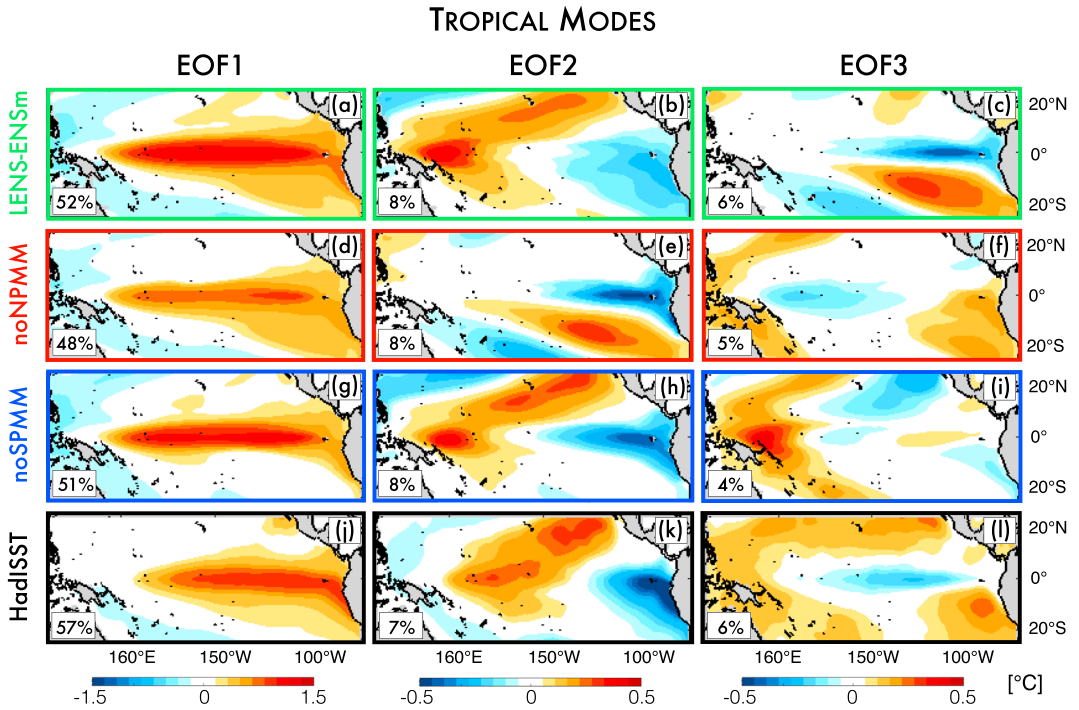

Figure 3. First three leading modes of tropical Pacific sea surface temperature anomalies ([120°E to 70°W, 25S° to 25°N]) in (a–c) LENS, (d–f) noNPMM, (g–i) noSPMM, and (j–l) HadISST v1.1. The numbers in the lower-left corner of each figure indicates the amount of explained variance, and units are in degrees Celsius. EOF = empirical orthogonal function; noNPMM = suppressed North Pacific Meridional Mode; noSPMM = suppressed South Pacific Meridional Mode; LENS = Large Ensemble.

significant differences in SST *SD* along equator (Figure 4a). However, separating the SST variability in an interannual (<8 years) and a decadal (>8 years) component suggests a more complex situation (Figures 4b and 4c). While suppression of the SPMM (i.e., noSPMM) does not impact the interannual tropical variance, it leads to a significant reduction in the decadal-scale variability. In contrast, the suppression of the NPMM (i.e., noNPMM) reduces significantly the interannual variability (Figure 4b) but not the decadal variability (Figure 4c). For a view of the El Niño cycle in both experiments and LENS, see the Figure S3 in the supporting information.

5. Impacts of NPMM and SPMM on TPDV

The reduction of the decadal-scale equatorial variance in the noSPMM experiment (Figure 4c) is confirmed by the power spectrum of the Niño3.4 index (Figure 4d), which shows a sharp decrease in the power for periods longer than about 4 years. Such a sharp decrease in low-frequency energy is not as clear in the power spectrum of the noNPMM experiment, which presents instead a broad-spectrum weakening including a strong suppression of the ENSO band (3–7 years; Figure 4c; see also the normalized power spectrum of Figure S4). To further characterize the role of meridional mode dynamics on the TPDV, we looked at the basin signature of the TPDV in both experiments and LENS. After applying an 8-year low-pass filter to the SSTa, we perform an EOF decomposition in the tropical Pacific sector that is not affected by the restoring ([10°S to 10°N]) to extract the decadal-scale climate signal.

The first EOF mode, which represent the TPDV, explains most of the low-frequency variance (85%, 90%, and 73%, in LENS, noNPMM and noSPMM, respectively) and is statistically distinct from higher-order modes (North et al., 1982). Excluding the region where the SST restoring is applied, the spatial signature of the TPDV that is obtained by regressing the PC1 onto the monthly SSTa over the entire Pacific basin reveals the characteristic equatorially symmetric pattern of ENSO-like decadal variability (Y. Zhang et al., 1997) in both LENS and noNPMM (Figures 4e and 4f) but not in the noSPMM (Figure 4g), which present

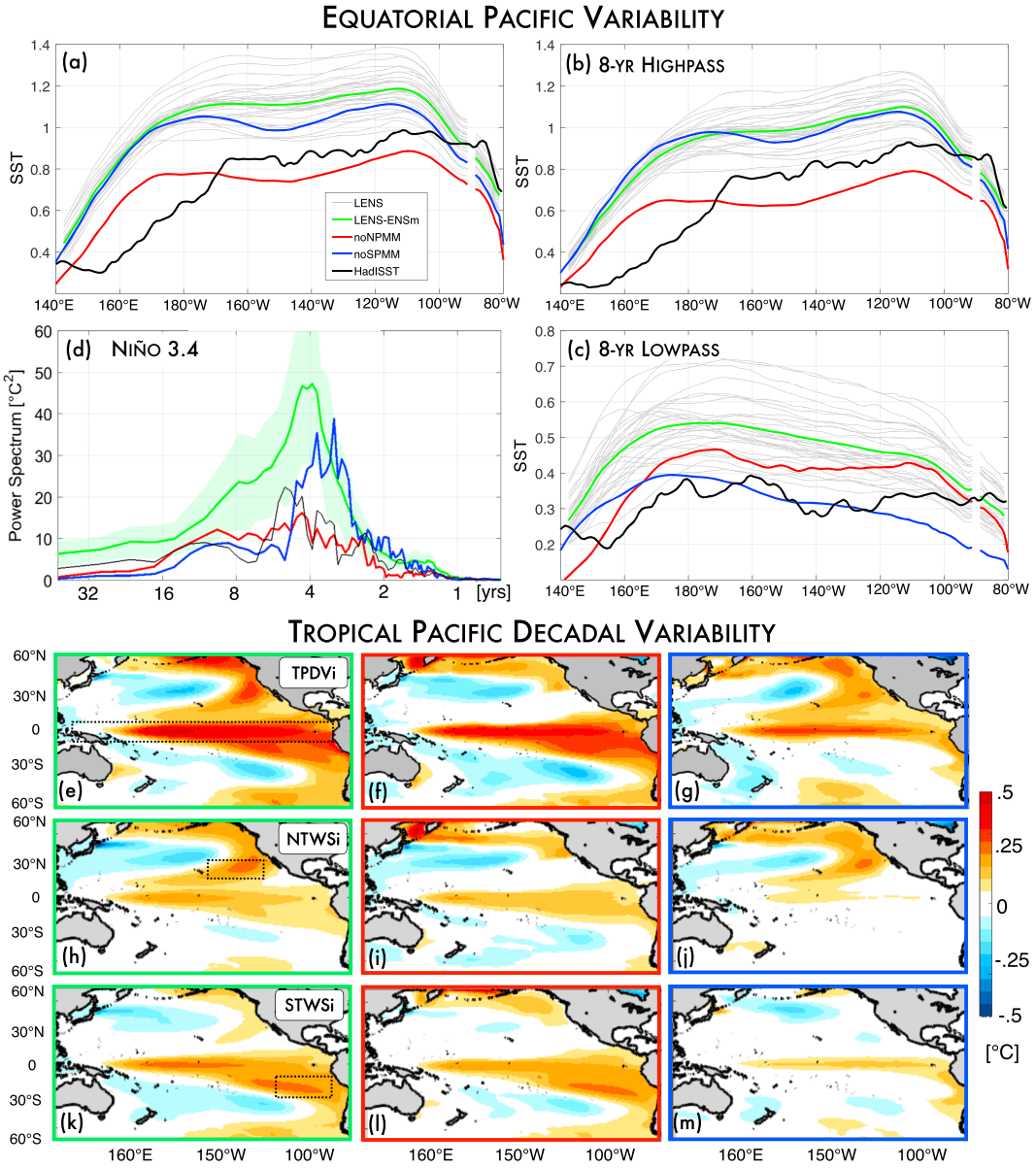

Figure 4. (a) Standard deviation in degrees Celsius, *SD*, of the monthly mean SSTa along the equatorial line (i.e., latitudinally averaged between 3°S and 3°N) for each LENS members (gray), LENS ensemble mean (green), noNPMM (red), noSPMM (blue), and HadISST v1.1 (black). (b, c) As in (a) but for interannual (i.e., 8-year high passed) and decadal (i.e., 8-year low passed) SSTa. (d) Power spectrum in degrees Celsius squared of Niño 3.4 index for LENS ensemble mean (green; shading indicates 1 SD spread envelope), noNPMM (red), noSPMM (blue), HadISST v1.1 (black). (e, h, and k) LENS 8-year low-passed SSTa regressed upon (e) the tropical Pacific decadal variability index (i.e., PC1 of 8-year low-passed SSTa over [10°S to 10°N]), (h) the northeasterly trade winds strength index (i.e., 8-year low-passed wind speed averaged over [150–120°W, 15–25°N]), and (k) the southeasterly trade winds strength index (i.e., 8-year low-passed wind speed averaged over [110–80°W, 25–15°S]). The same analysis is repeated for (f, i, and l) noNPMM and (g, j, and m) noSPMM experiments. LENS = Large Ensemble; noSPMM = suppressed South Pacific Meridional Mode; noNPMM = suppressed North Pacific Meridional Mode; SSTa = sea surface temperature anomalies.

substantially weaker anomalies in the tropics and important spatial differences in the Southern Hemisphere. Excluding the region where the SST restoring is applied, the spatial signature of the TPDV in LENS and noNPMM are similar in both hemispheres while the one of noSPMM differs substantially in the Southern Hemisphere. Specifically, the noSPMM lacks the negative anomaly pole centered at about [35°S, 110°W], the positive anomaly near eastern side of the Australian continent and the positive anomaly band in the extratropics that extends longitudinally from 140°W to the South America coastline.

6. Summary and Discussion of Mechanisms

Using observational data for SST and SLP over the period 1950–2005, we show that a significant fraction (~37% for SST and ~35% for SLP) of the late-fall (i.e., OND) interannual variability in the tropical Pacific, which is largely dominated by ENSO, can be explained by the state of the atmosphere (i.e., SLP) and ocean (i.e., SST) in the extratropics 9-month prior (i.e., JFM mean; Figures 1g and 1h). Although these prior SST and SLP conditions (i.e., ENSO precursors) are characterized by the signature of both the NPMM in the north and the SPMM in south (Figures 1a and 1c), the contribution of each meridional mode to the tropical Pacific variability differs substantially. Experiments with the CESM model reveals that the SPMM does not have a significant impact on the interannual statistics of the tropical Pacific while the NPMM plays a key role in initiating ENSO. Moreover, in CESM most of the tropical Pacific variability (~65%) is explained by the first three leading EOF modes, which generally track ENSO, the NPMM, and the SPMM, respectively. While the SPMM has a weak influence on ENSO and explains only ~6% of the TPV, it plays a key role in the decadal statistics of the Tropical Pacific. This finding provides an alternative hypothesis for the generation of TPDV, which previous studies have ascribed to residual variability of ENSO (e.g., Vimont, 2005) or to local coupled ocean-atmosphere dynamics in the tropical and North Pacific region (Liu et al., 2002). Further support for the idea that ENSO dynamics is not the primary source of TPDV is revealed by the experiment where the NPMM is suppressed, which leads to weaker ENSO but no significant decrease in the TPDV.

These results confirm a more recent view proposed by Okumura (2013) and consistent with observational analyses (Deser et al., 2004; Garreaud & Battisti, 1999) and modeling studies (Clement et al., 2011; Matei et al., 2008) in which the TPDV is tightly linked to the South Pacific. Specifically, Okumura (2013) proposed that the latitudinal asymmetry of the central and eastern tropical Pacific climate, with the intertropical convergence zone displaced north of the equator during most of the year, allows the extratropical atmospheric variability to drive SST changes in the southeast equatorial Pacific by modulating the intensity of the southeasterly trade winds. Moreover, the stronger impact of SPMM on decadal timescales could be explained by the dominant role of thermodynamic air-sea interactions, for which persistent intrusion of surface wind anomalies into the equatorial region is important. Differently, the NPMM may be effective in exciting equatorial oceanic waves and ENSO events through changes in subtropical winds during limited seasons, which may have little impact on the mean state of the tropical Pacific. The important role of the southeasterly trade winds in the TPDV is somewhat evident in LENS. Regression maps of 8-year low-passed SSTa with indices of the northeasterly and southeasterly trade winds strength (NTWSi and STWSi; Figure 4) reveal that the STWSi presents a larger signal in the Tropics that resemble more closely the TPDV pattern (Figure 4e). Repeating this analysis for noNPMM and noSPMM experiments confirms LENS results and suggests a negligible constructive interference between south and north precursors (Figures 4i, 4j, 4l, and 4m). Specifically, the suppression of the SST variability in the NPMM region results in southeasterly trade winds with a TPDV signature similar in shape and size of the anomaly to the ones in LENS (compare Figures 4k and 4l), suggesting a dominant and independent role of the south precursor in the TPDV. Although the noNPMM and noSPMM experiments helped revealing important characteristics of the two main extratropical ENSO precursors, the possibility that some results may be model dependent requires further confirmation in other climate models.

Acknowledgments
The authors thank Yuko Okumura for valuable contributions in the review process. They also thank an anonymous reviewer for constructive criticisms that improved the manuscript. G. L. thanks Taka Ito for the stimulating and insightful discussions and Pedro Di Nezio for his invaluable support with the CESM model and insightful discussion on the SST-restoring impact on ENSO. E. D. L. and G. L. acknowledge the support of the NSF-OCE 1634996 and NSF-OCE 1419292. G. L. was partially supported by the Domenica Rea D'Onofrio Fellowship and the ARC Centre of Excellence for Climate Extremes (grant CE170100023). We thank the National Center for Atmospheric Research for producing and making available the results from the CESM Large Ensemble Project http://www.cesm.ucar.edu/projects/community-projects/LENS/data-sets.html. Observational SST data were obtained from https://www.esrl.noaa.gov/psd/data/gridded/data.noaa.ersst.v3.html (ERSSTv3) and https://www.metoffice.gov.uk/hadobs/hadisst/data/download.html (HadISST).

References

Adams, R. M., Chen, C. C., McCarl, B. A., & Weiher, R. F. (1999). The economic consequences of ENSO events for agriculture. *Climate Research*, *13*(3), 165–172. https://doi.org/10.3354/cr013165

Alexander, M. A., Blade, I., Newman, M., Lanzante, J. R., Lau, N. C., & Scott, J. D. (2002). The atmospheric bridge: The influence of ENSO teleconnections on air-sea interaction over the global oceans. *Journal of Climate*, *15*(16), 2205–2231. https://doi.org/10.1175/1520-0442(2002)015<2205:TABTIO>2.0.CO;2

Alexander, M. A., Vimont, D. J., Chang, P., & Scott, J. D. (2010). The impact of extratropical atmospheric variability on ENSO: Testing the seasonal footprinting mechanism using coupled model experiments. *Journal of Climate*, *23*(11), 2885–2901. https://doi.org/10.1175/2010JCLI3205.1

Anderson, B. T. (2003). Tropical Pacific sea-surface temperatures and preceding sea level pressure anomalies in the subtropical North Pacific. *Journal of Geophysical Research*, *108*(D23), 4732. https://doi.org/10.1029/2003JD003805

Anderson, B. T., Perez, R. C., & Karspeck, A. (2013). Triggering of El Nino onset through trade wind-induced charging of the equatorial Pacific. *Geophysical Research Letters*, *40*, 1212–1216. https://doi.org/10.1002/grl.50200

Berry, B. J. L., & Okulicz-Kozaryn, A. (2008). Are there ENSO signals in the macroeconomy? *Ecological Economics*, *64*(3), 625–633. https://doi.org/10.1016/j.ecolecon.2007.04.009

Bjerknes, J. (1969). Atmospheric teleconnections from equatorial Pacific. *Monthly Weather Review*, *97*(3), 163–172. https://doi.org/10.1175/1520-0493(1969)097<0163:ATFTEP>2.3.CO;2

Cashin, P., Mohaddes, K., & Raissi, M. (2017). Fair weather or foul? The macroeconomic effects of El Nino. *Journal of International Economics*, *106*, 37–54. https://doi.org/10.1016/j.jinteco.2017.01.010

Chang, P., Zhang, L., Saravanan, R., Vimont, D. J., Chiang, J. C. H., Ji, L., et al. (2007). Pacific meridional mode and El Nino-Southern Oscillation. *Geophysical Research Letters*, *34*, L16608. https://doi.org/10.1029/2007GL030302

Chiang, J. C. H., & Vimont, D. J. (2004). Analogous Pacific and Atlantic meridional modes of tropical atmosphere-ocean variability. *Journal of Climate*, *17*(21), 4143–4158. https://doi.org/10.1175/JCLI4953.1

Clement, A., DiNezio, P., & Deser, C. (2011). Rethinking the ocean's role in the Southern Oscillation. *Journal of Climate*, *24*(15), 4056–4072. https://doi.org/10.1175/2011JCLI3973.1

Deser, C., Phillips, A. S., & Hurrell, J. W. (2004). Pacific interdecadal climate variability: Linkages between the tropics and the North Pacific during boreal winter since 1900. *Journal of Climate*, *17*(16), 3109–3124. https://doi.org/10.1175/1520-0442(2004)017<3109:PICVLB>2.0.CO;2

Di Lorenzo, E., Liguori, G., Schneider, N., Furtado, J. C., Anderson, B. T., & Alexander, M. A. (2015). ENSO and meridional modes: A null hypothesis for Pacific climate variability. *Geophysical Research Letters*, *42*, 9440–9448. https://doi.org/10.1002/2015GL066281

Ding, R. Q., Li, J. P., & Tseng, Y. H. (2015). The impact of South Pacific extratropical forcing on ENSO and comparisons with the North Pacific. *Climate Dynamics*, *44*(7–8), 2017–2034. https://doi.org/10.1007/s00382-014-2303-5

Fedorov, A. V. (2002). The response of the coupled tropical ocean-atmosphere to westerly wind bursts. *Quarterly Journal of the Royal Meteorological Society*, *128*(579), 1–23. https://doi.org/10.1002/qj.200212857901

Fisman, D. N., Tuite, A. R., & Brown, K. A. (2016). Impact of El Nino Southern Oscillation on infectious disease hospitalization risk in the United States. *Proceedings of the National Academy of Sciences of the United States of America*, *113*(51), 14,589–14,594. https://doi.org/10.1073/pnas.1604980113

Garreaud, R. D., & Battisti, D. S. (1999). Interannual (ENSO) and interdecadal (ENSO-like) variability in the Southern Hemisphere tropospheric circulation. *Journal of Climate*, *12*(7), 2113–2123. https://doi.org/10.1175/1520-0442(1999)012<2113:IEAIEL>2.0.CO;2

Harrison, D. E., & Larkin, N. K. (1998). El Nino-Southern Oscillation sea surface temperature and wind anomalies, 1946-1993. *Reviews of Geophysics*, *36*, 353–399. https://doi.org/10.1029/98RG00715

Hurrell, J. W., Holland, M. M., Gent, P. R., Ghan, S., Kay, J. E., Kushner, P. J., et al. (2013). The community Earth system model a framework for collaborative research. *Bulletin of the American Meteorological Society*, *94*(9), 1339–1360. https://doi.org/10.1175/BAMS-D-12-00121.1

Jin, F. F. (1997). An equatorial ocean recharge paradigm for ENSO.1. Conceptual model. *Journal of the Atmospheric Sciences*, *54*(7), 811–829. https://doi.org/10.1175/1520-0469(1997)054<0811:AEORPF>2.0.CO;2

Kessler, W. S., & Kleeman, R. (2000). Rectification of the Madden-Julian oscillation into the ENSO cycle. *Journal of Climate*, *13*(20), 3560–3575. https://doi.org/10.1175/1520-0442(2000)013<3560:ROTMJO>2.0.CO;2

Kistler, R., Collins, W., Saha, S., White, G., Woollen, J., Kalnay, E., et al. (2001). The NCEP-NCAR 50-year reanalysis: Monthly means CD-ROM and documentation. *Bulletin of the American Meteorological Society*, *82*(2), 247–267. https://doi.org/10.1175/1520-0477(2001)082<0247:TNNYRM>2.3.CO;2

Knutson, T. R., & Manabe, S. (1998). Model assessment of decadal variability and trends in the tropical Pacific Ocean. *Journal of Climate*, *11*(9), 2273–2296. https://doi.org/10.1175/1520-0442(1998)011<2273:MAODVA>2.0.CO;2

Larson, S., & Kirtman, B. (2013). The Pacific Meridional Mode as a trigger for ENSO in a high-resolution coupled model. *Geophysical Research Letters*, *40*, 3189–3194. https://doi.org/10.1002/grl.50571

Larson, S., & Kirtman, B. (2014). The Pacific Meridional Mode as an ENSO precursor and predictor in the North American multimodel ensemble. *Journal of Climate*, *27*(18), 7018–7032. https://doi.org/10.1175/JCLI-D-14-00055.1

Liguori, G., & Di Lorenzo, E. (2018). Meridional modes and increasing Pacific decadal variability under anthropogenic forcing. *Geophysical Research Letters*, *45*, 983–991. https://doi.org/10.1002/2017GL076548

Linkin, M. E., & Nigam, S. (2008). The North Pacific Oscillation–West Pacific teleconnection pattern: Mature-phase structure and winter impacts. *Journal of Climate*, *21*(9), 1979–1997. https://doi.org/10.1175/2007JCLI2048.1

Liu, Z., Wu, L., Gallimore, R., & Jacob, R. (2002). Search for the origins of Pacific decadal climate variability. *Geophysical Research Letters*, *29*(10), 1404. https://doi.org/10.1029/2001GL013735

Matei, D., Keenlyside, N., Latif, M., & Jungclaus, J. (2008). Subtropical forcing of tropical Pacific climate and decadal ENSO modulation. *Journal of Climate*, *21*(18), 4691–4709. https://doi.org/10.1175/2008JCLI2075.1

McPhaden, M. J. (1999). Genesis and evolution of the 1997-98 El Nino. *Science*, *283*(5404), 950–954. https://doi.org/10.1126/science.283.5404.950

McPhaden, M. J., & Yu, X. (1999). Equatorial waves and the 1997-98 El Nino. *Geophysical Research Letters*, *26*, 2961–2964. https://doi.org/10.1029/1999GL004901

McPhaden, M. J., Zebiak, S. E., & Glantz, M. H. (2006). ENSO as an integrating concept in Earth science. *Science*, *314*(5806), 1740–1745. https://doi.org/10.1126/science.1132588

North, G. R., Bell, T. L., Cahalan, R. F., & Moeng, F. J. (1982). Sampling errors in the estimation of empirical orthogonal functions. *Monthly Weather Review*, *110*(7), 699–706. https://doi.org/10.1175/1520-0493(1982)110<0699:SEITEO>2.0.CO;2

Okumura, Y. M. (2013). Origins of tropical Pacific decadal variability: Role of stochastic atmospheric forcing from the South Pacific. *Journal of Climate*, *26*(24), 9791–9796. https://doi.org/10.1175/JCLI-D-13-00448.1

Rayner, N. A., Parker, D. E., Horton, E. B., Folland, C. K., Alexander, L. V., Rowell, D. P., et al. (2003). Global analyses of sea surface temperature, sea ice, and night marine air temperature since the late nineteenth century. *Journal of Geophysical Research*, *108*(D14), 4407. https://doi.org/10.1029/2002JD002670

Rogers, J. C. (1981). The North Pacific Oscillation. *Journal of Climatology*, *1*(1), 39–57. https://doi.org/10.1002/joc.3370010106

Smith, T. M., & Reynolds, R. W. (2005). A global merged land-air-sea surface temperature reconstruction based on historical observations (1880-1997). *Journal of Climate*, *18*(12), 2021–2036. https://doi.org/10.1175/JCLI3362.1

Suarez, M. J., & Schopf, P. S. (1988). A delayed action oscillator for ENSO. *Journal of the Atmospheric Sciences*, *45*(21), 3283–3287. https://doi.org/10.1175/1520-0469(1988)045<3283:ADAOFE>2.0.CO;2

Thomas, E. E., & Vimont, D. J. (2016). Modeling the mechanisms of linear and nonlinear ENSO responses to the Pacific Meridional Mode. *Journal of Climate*, *29*(24), 8745–8761. https://doi.org/10.1175/JCLI-D-16-0090.1

Vimont, D. J. (2005). The contribution of the interannual ENSO cycle to the spatial pattern of decadal ENSO-like variability. *Journal of Climate*, *18*(12), 2080–2092. https://doi.org/10.1175/JCLI3365.1

Vimont, D. J., Battisti, D. S., & Hirst, A. C. (2001). Footprinting: A seasonal connection between the tropics and mid-latitudes. *Geophysical Research Letters*, *28*, 3923–3926. https://doi.org/10.1029/2001GL013435

Vimont, D. J., Wallace, J. M., & Battisti, D. S. (2003). The seasonal footprinting mechanism in the Pacific: Implications for ENSO. *Journal of Climate*, *16*(16), 2668–2675. https://doi.org/10.1175/1520-0442(2003)016<2668:TSFMIT>2.0.CO;2

Wang, X. C., Jin, F. F., & Wang, Y. Q. (2003). A tropical ocean recharge mechanism for climate variability. Part I: Equatorial heat content changes induced by the off-equatorial wind. *Journal of Climate*, *16*(22), 3585–3598. https://doi.org/10.1175/1520-0442(2003)016<3585:ATORMF>2.0.CO;2

Xie, S. P., & Philander, S. G. H. (1994). A coupled ocean-atmosphere model of relevance to the ITCZ in the eastern Pacific. *Tellus A*, *46*(4), 340–350. https://doi.org/10.3402/tellusa.v46i4.15484

You, Y. J., & Furtado, J. C. (2017). The role of South Pacific atmospheric variability in the development of different types of ENSO. *Geophysical Research Letters*, *44*, 7438–7446. https://doi.org/10.1002/2017GL073475

Zavala-Garay, J., Zhang, C., Moore, A. M., & Kleeman, R. (2005). The linear response of ENSO to the Madden-Julian oscillation. *Journal of Climate*, *18*(13), 2441–2459. https://doi.org/10.1175/JCLI3408.1

Zhang, H., Clement, A., & Di Nezio, P. (2014). The South Pacific Meridional Mode: A mechanism for ENSO-like variability. *Journal of Climate*, *27*(2), 769–783. https://doi.org/10.1175/JCLI-D-13-00082.1

Zhang, L., Chang, P., & Ji, L. (2009). Linking the Pacific Meridional Mode to ENSO: Coupled model analysis. *Journal of Climate*, *22*(12), 3488–3505. https://doi.org/10.1175/2008JCLI2473.1

Zhang, L., Chang, P., & Tippett, M. K. (2009). Linking the Pacific Meridional Mode to ENSO: Utilization of a noise filter. *Journal of Climate*, *22*(4), 905–922. https://doi.org/10.1175/2008JCLI2474.1

Zhang, Y., Wallace, J. M., & Battisti, D. S. (1997). ENSO-like interdecadal variability: 1900-93. *Journal of Climate*, *10*(5), 1004–1020. https://doi.org/10.1175/1520-0442(1997)010<1004:ELIV>2.0.CO;2